Available online at www.sciencedirect.com
ScienceDirect
Materials Research Bulletin 42 (2007) 1440–1449
Materials Research Bulletin
www.elsevier.com/locate/matresbu

Europium-doped yttrium silicate nanophosphors prepared by flame synthesis

Xiao Qin [a,*], Yiguang Ju [a], Stefan Bernhard [b], Nan Yao [c]

[a] Department of Mechanical and Aerospace Engineering, Princeton University, Princeton, NJ 08544, United States
[b] Department of Chemistry, Princeton University, Princeton, NJ 08544, United States
[c] Princeton Institute for the Science and Technology of Materials, Princeton University, Princeton, NJ 08544, United States

Received 18 August 2006; received in revised form 14 October 2006; accepted 7 November 2006
Available online 22 December 2006

Abstract

Europium-doped yttrium silicate ($Y_2SiO_5:Eu^{3+}$) nanophosphors were successfully synthesized by flame spray pyrolysis method. The effect of silicon concentration on the crystal structure and morphology of the $Y_2SiO_5:Eu^{3+}$ phosphors were investigated. As-prepared phosphor consists of spherical nanoparticles with filled morphology, high crystallinity, narrow size distribution, and intense photoluminescence. The crystal structure and photoluminescence intensity of $Y_2SiO_5:Eu^{3+}$ nanophosphors are strongly affected by the ratio of silicon to yttrium in the precursor solution, and the maximum photoluminescence intensity is obtained from particles prepared from the silicon to yttrium ratio of 1.25. A concentration quenching limit is observed at 30 mol% Eu of yttrium. The photoluminescence intensity also increases with the increase of the concentration of precursor solution. This work demonstrates the advantages of flame spray pyrolysis method for the preparation of multi-component nanophosphor, which can be found potential application in lamp and display industries.

Keywords: A. Inorganic compounds; C. X-ray diffraction; D. Crystal structure; D. Optical properties

1. Introduction

Yttrium silicate (Y_2SiO_5) is an important luminescent host material for various rare-earth (RE) activators [1]. Its excellent thermal and chemical stability makes it a good laser host [2,3]. The Ce-activated Y_2SiO_5 is one of the best low-voltage blue phosphor in field emission displays (FED) due to its excellent luminescence efficiency, color purity and stability [4], while the Tb^{3+}-doped Y_2SiO_5 is one of the best green emitting cathodoluminescent phosphors [5]. On the other hand, $Y_2SiO_5:Eu^{3+}$, with its sharp emission in red, is considered as a promising phosphor for high resolution displays [6] because the red component of the three color centers is the most important part when considering susceptibility of human eye. Moreover, $Y_2SiO_5:Eu^{3+}$ was also found to be a promising candidate for coherent time-domain optical memory applications [7]

There are two types of Y_2SiO_5 crystal: monoclinic X_1-type (crystallographic group $P2_1/c$) and monoclinic X_2-type (crystallographic group $B2/b$) [8,9]. The X_1- and X_2-types can be formed by varying the synthesis temperature. The high-temperature synthesis leads to the X_2-type and low-temperature synthesis to the X_1-type [10]. The X_2-Y_2SiO_5 is a

* Corresponding author. Tel.: +1 609 258 1411; fax: +1 609 258 6123.
E-mail address: xqin@princeton.edu (X. Qin).

0025-5408/$ – see front matter © 2006 Elsevier Ltd. All rights reserved.
doi:10.1016/j.materresbull.2006.11.021

better host lattice for the luminescence of lanthanide ions than the X_1-Y_2SiO_5 [1,9]. The host lattice of X_2-Y_2SiO_5 is stiffer than that of X_1-Y_2SiO_5 because of the higher formation temperature of X_2-Y_2SiO_5 and has lower coordination number in it. According to the model of Verwey and Blasse [11], since the host lattice of X_1-Y_2SiO_5 is not as rigid as that of X_2-Y_2SiO_5, the expansion after excitation is less restricted by the surrounding of the luminescent ions in the former than in the latter. As a result, more nonradiative relaxations take place in X_1-Y_2SiO_5 than in X_2-Y_2SiO_5.

In general, the rare-earth-doped yttrium silicate phosphors are synthesized by the solid-state reaction of Y_2O_3, SiO_2 and activators at high temperature [4]. However, this method requires a high processing temperature, a long processing time, repeated milling and washing with chemicals. These processes tend to degrade the luminescence efficiency of the phosphor and yield particles with irregular shape. Sol–gel method has been employed to synthesize Y_2SiO_5:RE^{3+} phosphors by some researchers [12–15]. The as-prepared powders have low crystallinity and require heat-treatment at high temperature, which results in severe agglomerations. Conventional spray pyrolysis was also used to prepare Y_2SiO_5:Ce^{3+} and Y_2SiO_5:Tb^{3+} particles with spherical morphology [16,17]. The problem with this preparation technique is the formation of hollow and porous particles which are not desirable for efficient phosphors. Also, spray-pyrolysis-produced powders require high temperature post-synthesis treatment for crystallization and activation of phosphor particles.

Recently, flame spray pyrolysis technique was successfully applied for the synthesis of europium-doped yttrium nanoparticles [18–21]. This synthesis technique is very promising for a broad spectrum of functional nanoparticles [18–21]. The use of combustion can avoid hollowness and provide the high temperature environment favorable to phosphor synthesis. The flame temperature and the residence time of particles in the flame, which are very important parameters determining particle characteristics, can be easily controlled by varying fuel and oxidizer flow rates. The particle size can be controlled by varying precursor solution concentration while multi-component particles can be obtained by adding different salts into the solution [22]. Moreover, this technique can be easily scaled up for the manufacture of commercial quantities of nanoparticles [23]. However, there is no report available on the flame synthesis of Y_2SiO_5:Eu^{3+} nanophosphors, and the relationship between the flame and nanophosphor properties is not well understood.

The objective of this work is to explore the flame synthesis method for the preparation of Y_2SiO_5:Eu^{3+} phosphor in a form of spherical nanoparticles with dense structure and high photoluminescence intensity. The effects of silicon and europium concentration on the crystal structure, particle morphology and size, and photoluminescence intensity of the as-prepared and heat-treated particles were also investigated.

2. Experimental

The details of the flame spray pyrolysis system used in this work are given in our previous study of europium-doped yttria nanoparticles [18]. The system consists of a spray generator, a coflow burner, a quartz reactor, particle collection filters and a vacuum pump. An ultrasonic spray generator operating at 1.7 MHz is used to generate fine spray droplets which are then carried into the flame by nitrogen gas though a central tube. The advantage of an ultrasonic nebulizer in atomizing liquid precursors is that fine sprays can be obtained with a narrow droplet size distribution in the range of 1–10 μm [24]; while atomizing nozzles (both air-assisted type and pressure type) generate droplets with diameters between 1 and 200 μm [21]. The flame nozzle consists of three concentric stainless steel tubes. A methane and oxygen nonpremixed flame is used for the flame synthesis. The typical flow rates of nitrogen, methane and oxygen gases are 0.3, 0.3, and 1.5 L/min, respectively, which results in an adiabatic flame temperature of 2628 K. Here, the adiabatic flame temperature at equilibrium state is calculated using the CHEMKIN II package [25], where CH_4, O_2, N_2 are considered as reactants and CH_4, O_2, N_2, H_2O, CO_2, CO, H, H_2, OH, O, N, NO, and NO_2 as products.

The starting materials of tetraethyl orthosilicate [TEOS, $(C_2H_5O)_4Si$, 99.9%, Alfa Aesar], yttrium and europium nitrate [$Y(NO_3)_3{\cdot}6H_2O$, 99.99%, $Eu(NO_3)_3{\cdot}6H_2O$, 99.99%, Alfa Aesar] are dissolved in ethyl alcohol. The europium doping concentration (represented by x, which is the mole fraction of Eu in $Y_{2-x}Eu_xSiO_5$) is varied from 0.1 to 0.7 (or 5–35 mol% Eu of Y). The ratio of silicon (TEOS) to yttrium in the precursor is defined as the equivalence ratio of silicon (TEOS), $\phi = (X_{TEOS}/X_Y)/(X_{TEOS}/X_Y)_{stoi}$, where X is the mole fraction. The overall concentration (C) of the precursor solution is varying from 0.001 to 0.5 M in order to obtain particles of different size.

The particles are collected using a micron glassfiber filter (Whatmann GF/F) located 30 cm above the flame. Powder X-ray diffractometer (XRD, 30 kV and 20 mA, Cu Kα, Rigaku) is used for crystal phase identification and estimation of the crystallite size. The powders are pasted on a quartz glass and the scan is performed in the 2θ range of

10–60°. The morphology and size of particles was examined using a field-emission scanning electron microscope (FE-SEM, Philips XL30). The photoluminescence spectra are measured with a Jobin-Yvon Fluorolog-3 fluorometer equipped with a front face detection setup and two double monochromators. The samples are excited with a 150 W Xenon lamp and a 2 nm slit width is used for both monochromators. All samples are examined at room temperature. A commercial trichromatic lamp phosphor (Y_2O_3:Eu, Stanford Materials) is used as the reference system for the photoluminescence measurements.

3. Results and discussion

Fig. 1 shows the scanning electron micrographs of the as-prepared $Y_2SiO_5:Eu^{3+}$ phosphors at different ratios of silicon to yttrium (equivalence ratio ϕ), europium concentration and overall precursor concentration. For the as-prepared samples constituting particles are spherical, non-agglomerated, and with narrow size distribution (Fig. 1a–e). Differently, the commercial lamp phosphors (Y_2O_3:Eu) prepared by solid state reaction have particles with irregular shape and strongly agglomerated (Fig. 1f). The mean particle size decreases with the decrease of the overall precursor

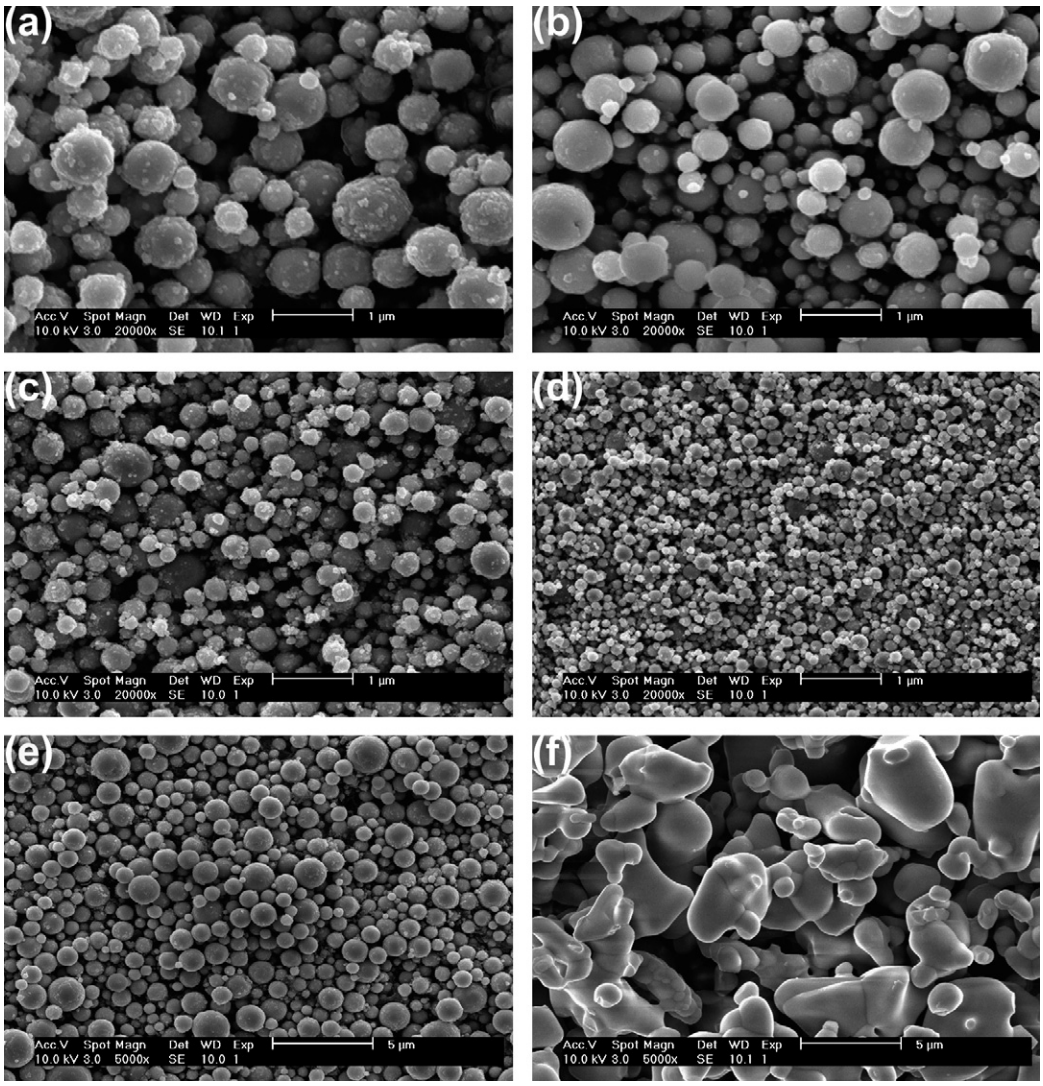

Fig. 1. SEM images of as-prepared $Y_{2-x}Eu_xSiO_5$ samples of different overall precursor concentration and Eu concentration: (a) 0.1 M, $\phi = 1.0$, $x = 0.1$; (b) 0.1 M, $\phi = 1.25$, $x = 0.6$; (c) 0.01 M, $\phi = 1.25$, $x = 0.1$; (d) 0.001 M, $\phi = 1.25$, $x = 0.1$; (e) 0.5 M, $\phi = 1.25$, $x = 0.6$; (f) commercial Y_2O_3:Eu. The scale bar is 1 μm in (a)–(d) and 5 μm in (e) and (f).

concentration. For the samples prepared from the precursor solution at $\phi = 1.25$ and $x = 0.1$, the average diameter (obtained from the average of 500 particles in the SEM images) is 915, 544, 237 and 136 nm, respectively, for the concentration of 0.5, 0.1, 0.01, and 0.001 M. It should be noticed that there is little effect on the particle morphology and size by changing the equivalence ratio of TEOS in the precursor solution or the europium concentration at a given overall precursor concentration. For example, when the precursor concentration is 0.1 M, the mean particle diameter is 544 nm for the sample prepared from $\phi = 1.0$ and $x = 0.1$ solution (Fig. 1a), 549 nm from $\phi = 1.25$ and $x = 0.6$ solution (Fig. 1b), and 537 nm for $\phi = 1.5$ and $x = 0.1$ solution (not shown here). The average particle size of the commercial phosphor is 4.1 μm. Fig. 2 shows the histograms of particle size distribution corresponding to samples in Fig. 1a, c and d.

The crystal structure of the as-prepared and heat-treated $Y_2SiO_5:Eu^{3+}$ phosphors are examined by XRD and obtained spectra are shown in Fig. 3. As mentioned previously, Y_2SiO_5 is polymorphic and crystallizes in the monoclinic X_1- or X_2-type at different synthesis temperature. The XRD spectra in Fig. 3a–d show that the as-prepared $Y_2SiO_5:Eu^{3+}$ samples have an X_1-type crystal structure, which was confirmed by comparing with the diffraction data of JCPDS card 21-1456 (indicated by the symbol (■) in Fig. 3b). Fig. 3e–g shows that after annealing at 1300 °C for 3 h, the X_1-type $Y_2SiO_5:Eu^{3+}$ samples transform to X_2-type. This is confirmed by the diffraction spectra of JCPDS card 21-1458 (indicated by the symbol (▼) in Fig. 3f). The average crystallite size can be calculated by Scherrer's equation: $D = 0.89\lambda/B \cos\theta$, where λ (=0.1540598 nm), θ and B are respectively the wavelength of the X-ray, the diffraction angle and the full width at half maximum (FWHM) of the XRD peaks (corresponding to 2θ), while 0.89 is a constant for spherical particles. The average crystallite size for the as-prepared X_1-Y_2SiO_5 is around 28 nm, and 41 nm for the heat-treated X_2-Y_2SiO_5.

The effect of silicon concentration with respect to yttrium on the crystal phase of X_1-Y_2SiO_5 was investigated. From Fig. 3a–d, it is seen that there are three different crystalline phases depending on the ratio of silicon to yttrium (silicon equivalence ratio). For silicon equivalence ratio less than 1.25, the XRD spectra (Fig. 3a) shows an incomplete crystalline phase of X_1-Y_2SiO_5. When the silicon equivalence ratio is increased to $\phi = 1.25$ or higher, the XRD spectra shows that a pure X_1-Y_2SiO_5 phase was obtained (Fig. 3b and c). As the silicon equivalence ratio further increases ($\phi \geq 2.0$), the XRD spectra (Fig. 3d) shows that an amorphous SiO_2 is dominant and the intensity of X_1-Y_2SiO_5 becomes much weak. Therefore, the ratio of silicon to yttrium in the precursor has a significant impact on the crystallity of the phosphors. When the silicon equivalence ratio is less than stoichiometry, excess amount of yttrium oxidizes into Y_2O_3 and coexists with Y_2SiO_5. On the other hand, when silicon is in excess amount with respect to yttrium, the remaining silicon forms SiO_2 which accounts for the amorphous background in the XRD spectra (see Fig. 3d).

Fig. 4 shows the excitation spectra of the X_1- and X_2-$Y_2SiO_5:Eu^{3+}$ samples under a wavelength of 613 nm. The intensity from the X_2-type particles is much stronger than from X_1-type, indicating that X_2-$Y_2SiO_5:Eu^{3+}$ is more efficient under UV excitation. On the other hand, both types of phosphors show a strong wide band between 200 and 350 nm with one small peak at 212 nm, and several sharp peaks between 350 and 600 nm. The strong wide band peaked at 258 nm is due to the charge-transfer (CT) transition in the Eu^{3+}–O^{2-} bond: an electron jumps from oxygen to europium [26]. The small peak at 212 nm is attributed to the host lattice (HL) absorption. The sharp peaks between 350 and 600 nm are due to electronic transitions within the nonbonding $4f^6$ shell of Eu^{3+}. Among the 4f–4f transitions, the most intense one corresponds to the electric dipole transition $^7F_0 \rightarrow {}^5L_6$ while the magnetic dipole transitions $^7F_1 \rightarrow {}^5D_2$ and $^7F_0 \rightarrow {}^5D_1$ are weaker. This is consistent with a noncentrosymmetric site provided by the monoclinic symmetry of the ligand arrangement.

Both as-prepared (X_1-type) and annealed (X_2-type) $Y_2SiO_5:Eu^{3+}$ samples exhibit red emissions under ultraviolet lamp irradiation at room temperature. Fig. 5 shows the emission spectra of X_1- and X_2-$Y_2SiO_5:Eu^{3+}$ phosphors excited at 355 nm. For comparison, the emission spectra of the commercial lamp phosphors (Y_2O_3:Eu) was also plotted in Fig. 5. The samples were prepared from a solution of an overall concentration of 0.1 M with $\phi = 1.25$ and $x = 0.6$. The photoluminescence (PL) measurements are normalized to the PL intensity of the commercial lamp phosphor Y_2O_3:Eu. Although the peak intensity of X_1- and X_2-$Y_2SiO_5:Eu^{3+}$ phosphors are only 24% and 57%, respectively, of the commercial Y_2O_3:Eu phosphor, their integral PL intensities are 112% and 126% in comparison to Y_2O_3:Eu. It should be noted that direct comparison between our products and the commercial Y_2O_3:Eu phosphor is not entirely appropriate, as they differ in composition, particle size and crystal structure. Also, the commercial product is optimized for a specific application. However, similar integral intensity between the investigated and the commercial products shows that both as-prepared and annealed $Y_2SiO_5:Eu^{3+}$ samples are good phosphors.

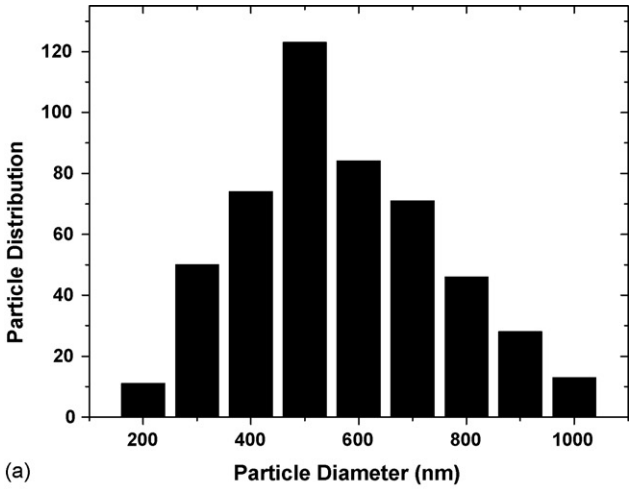

(a)

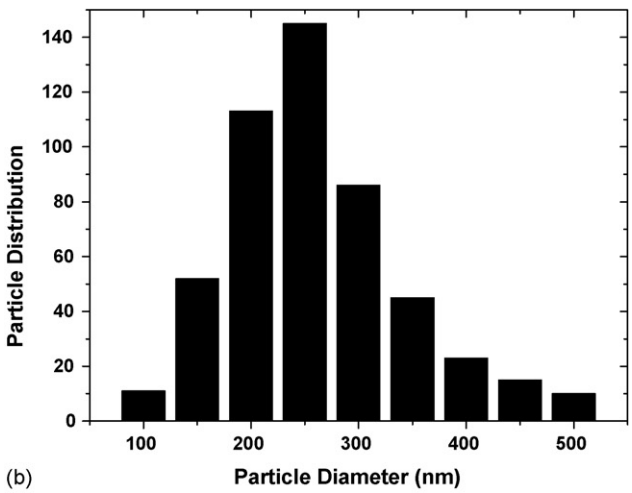

(b)

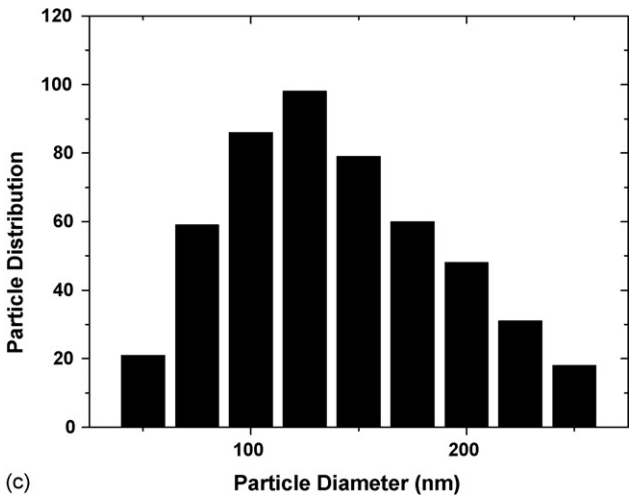

(c)

Fig. 2. Histograms of particle size distribution corresponding to samples in (a) Fig. 1a, (b) Fig. 1c and (c) Fig. 1d.

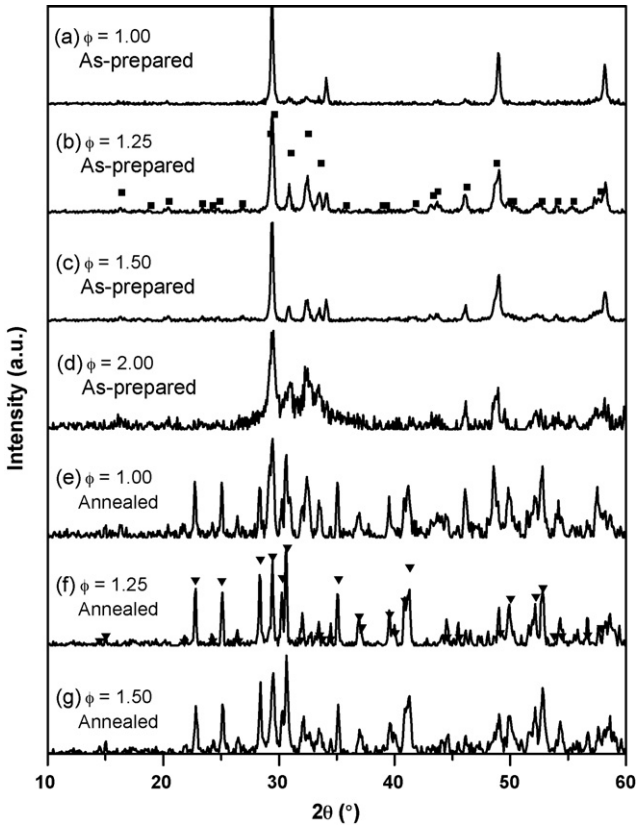

Fig. 3. XRD spectra of $Y_{1.9}Eu_{0.1}SiO_5$ samples prepared from different ratios of TEOS to yttrium nitrate: (a) ϕ = 1.0, as-prepared; (b) $\phi = 1.25$, as-prepared; (c) $\phi = 1.5$, as-prepared; (d) $\phi = 2.0$, as-prepared; (e) $\phi = 1.0$, annealed; (f) $\phi = 1.25$, annealed; (g) $\phi = 1.5$, annealed. The annealing treatment is done at 1300 °C for 3 h. The symbol (■) in (b) indicates the diffraction data of X_1-Y_2SiO_5 from JCPDS card 21-1456. The symbol (▼) in (f) indicates the diffraction data of X_2-Y_2SiO_5 from JCPDS card 21-1458.

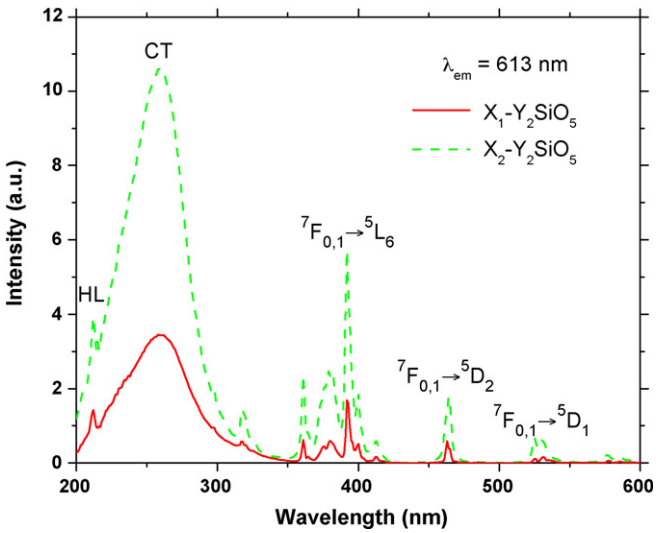

Fig. 4. Photoluminescence excitation spectra of X_1-type (as-prepared) and X_2-type (annealed at 1300 °C for 3 h) $Y_{2-x}Eu_xSiO_5$ ($x = 0.6$) samples. The overall precursor concentration is 0.1 M. Here, CT represents the charge-transfer transition in the Eu^{3+}–O^{2-} bond and HL means the host lattice absorption.

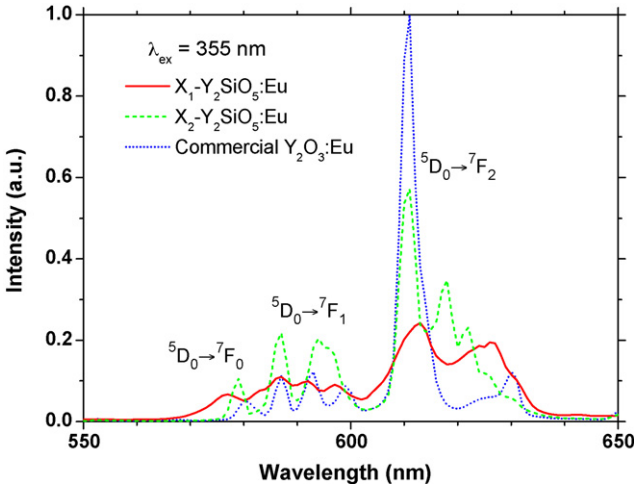

Fig. 5. Photoluminescence emission spectra of X_1-type (as-prepared) and X_2-type (annealed at 1300 °C for 3 h) $Y_{2-x}Eu_xSiO_5$ ($x = 0.6$) samples. The overall precursor concentration is 0.1 M.

For both X_1- and X_2-types of particles, all the intense fluorescence peaks originate in the $^5D_0$ state of Eu^{3+} and the strongest one is the hypersensitive electric dipole transition $^5D_0 \rightarrow {}^7F_2$. However, the spectral character and intensities of the two types of host lattices exhibit clear differences. In the X_1-Y_2SiO_5:Eu^{3+}, the emission spectrum of Eu^{3+} shows one $^5D_0 \rightarrow {}^7F_0$ peak (577 nm), four $^5D_0 \rightarrow {}^7F_1$ peaks (583, 587, 592, 597 nm), and four $^5D_0 \rightarrow {}^7F_2$ peaks (613, 623, 627, 631 nm), while in the X_2-Y_2SiO_5:Eu^{3+} there is only one $^5D_0 \rightarrow {}^7F_0$ peak (579 nm), three $^5D_0 \rightarrow {}^7F_1$ peaks (587, 594, 596 nm), and four $^5D_0 \rightarrow {}^7F_2$ peaks (611, 618, 622, 626 nm). From Fig. 4, it can be concluded that the flame spray pyrolysis exhibits a great advantage over other synthesis methods for preparing the X_1-type Y_2SiO_5:Eu^{3+} phosphors. In previous studies (sol–gel [15], spray pyrolysis [17], etc.), the as-prepared particles show poor crystalline structure and low luminescent intensities due to their low synthesis temperature. Further heat treatment up to 1100 °C is necessary for obtaining pure X_1-type crystal phase. In the present work, the as-prepared X_1-Y_2SiO_5:Eu^{3+} phosphors have a strong red luminescence and require no additional post-heat treatment, which greatly simplifies the manufacturing process and reduces the cost.

Fig. 6 shows the PL spectra of samples prepared at different Eu doping concentration. The emission intensity of the $Y_{2-x}Eu_xSiO_5$ particles is strongly affected by Eu doping concentration. Optimum intensity is obtained at a doping

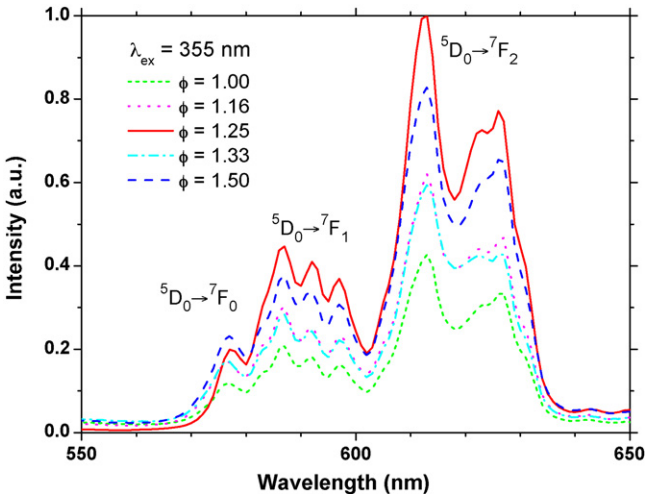

Fig. 6. PL spectra of X_1-$Y_{2-x}Eu_xSiO_5$ ($x = 0.6$) samples from different TEOS concentration. The overall precursor concentration is 0.1 M.

concentration of 30 mol% Eu to yttrium, which corresponds to $x = 0.6$ in the formula of $Y_{2-x}Eu_xSiO_5$. This value is larger than for bulk materials ($x = 0.2$) which have a larger size of crystallites [27]. The present result is in good agreement with that of Zhang et al. [13] who reported that the quenching concentration is $x = 0.6$ for sol–gel prepared nanocrystalline X_1-Y_2SiO_5:Eu^{3+}. For europium-doped phosphors, the quenching process is attributed to the energy migration among the activators (Eu^{3+} ions) which bring excitation energy to the nearby quenching centers (traps). These traps are usually trace impurities or defects on the particle. For bulk Y_2SiO_5:Eu^{3+} materials, when Eu concentration is low, the luminescent centers are isolated and only a few will transfer energy to the nearby traps. As the Eu concentration increases to $x = 0.2$, the luminescent centers are closer to each other in the crystal and energy can be rapidly transferred to a trap. As a result, most excited centers lose energy non-radiatively and thus concentration quenching occurs. On the other hand, in Y_2SiO_5:Eu^{3+} nanoparticles there are only a few traps that are randomly distributed in a particle due to the limited number of primitive cells. As the Eu concentration increases, quenching occurs first in particles containing many traps, while those particles containing few or no traps quench only at high concentration. Consequently, concentration quenching occurs at higher Eu concentrations in nanocrystalline Y_2SiO_5:Eu^{3+} than in bulk material.

Fig. 7 shows the emission spectra of the X_1-$Y_{2-x}Eu_xSiO_5$ ($x = 0.6$) phosphors prepared from different ratios of silicon to yttrium. The excitation wavelength is 355 nm and the overall precursor concentration is 0.1 M for all the cases. For the phosphors prepared at different silicon equivalence ratios, the spectrum characteristics (peak numbers and their locations) are same; however, the PL intensities are strongly affected by the silicon concentration. The maximum intensity occurs at the equivalence ratio of $\phi = 1.25$, with more than twice the intensity measured from the phosphors prepared from stoichiometric solution.

Fig. 8 shows the XRD spectra of the as-prepared samples obtained from precursor solutions of different overall concentrations. All samples exhibit an X_1-type crystal structure, which can be confirmed by comparing with the JCPDS card 21-1456 (indicated by drop lines in Fig. 7a). The peak intensity decreases with decreasing solution concentration. By Scherrer's equation, the average crystallite size is about 31 nm for the particles from 0.5 M solution, 28 nm for 0.1 M, and 27 nm for 0.01 M particles.

Fig. 9 shows the emission spectra of the as-prepared particles obtained from solutions of different overall concentrations. The luminescent intensity of the X_1-Y_2SiO_5:Eu^{3+} phosphors decrease as the particle size decreases. This may be attributed to the increase of crystallite size of larger particles prepared from high concentration precursors. The effect of particle size on the luminescent intensity is not clear yet. For example, Sharmar et al. [28] have reported that the emission intensity was increased about five times by reducing the Y_2O_3:Eu^{3+} particle size from 6 μm to 10 nm. But Hirai et al. [29] have reported that smaller particles show weaker emission intensities for their Y_2O_3:Eu^{3+} particle ranging from 60 to 200 nm. Further study is undergoing to investigate the particle size effect on the photoluminescence intensity in flame synthesis.

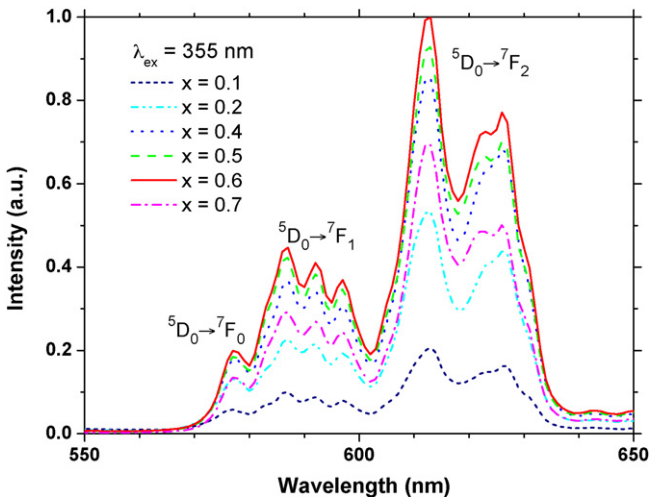

Fig. 7. PL spectra of X_1-$Y_{2-x}Eu_xSiO_5$ ($\phi = 1.25$) samples of different Eu doping concentration. The overall precursor concentration is 0.1 M.

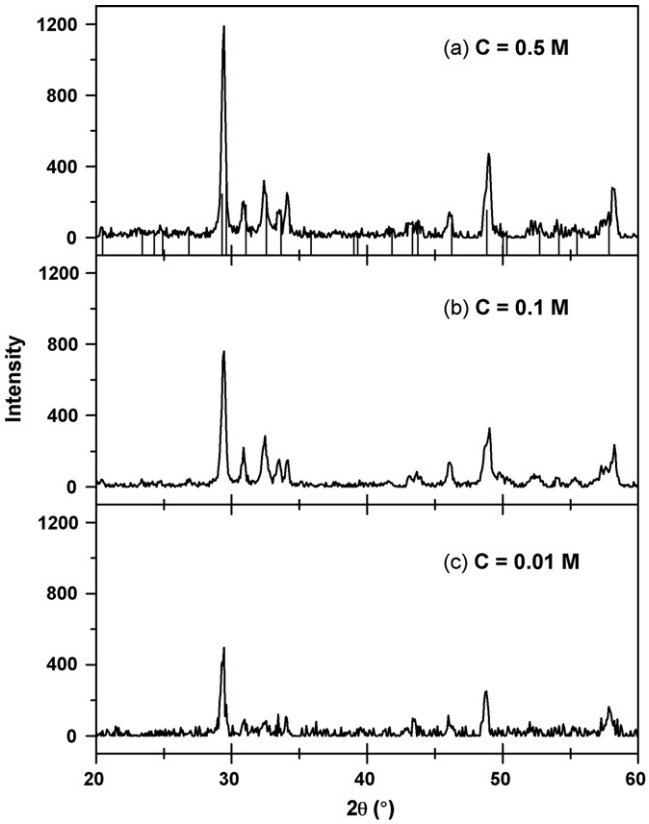

Fig. 8. XRD spectra of as-prepared X_1-Y_2SiO_5 samples from precursor solutions of different overall concentration of (a) 0.5 M, (b) 0.1 M and (c) 0.01 M. Other conditions are $\phi = 1.25$ and $x = 0.6$. The drop lines in (a) represents the peaks of X_1-Y_2SiO_5 from JCPDS card 21-1456.

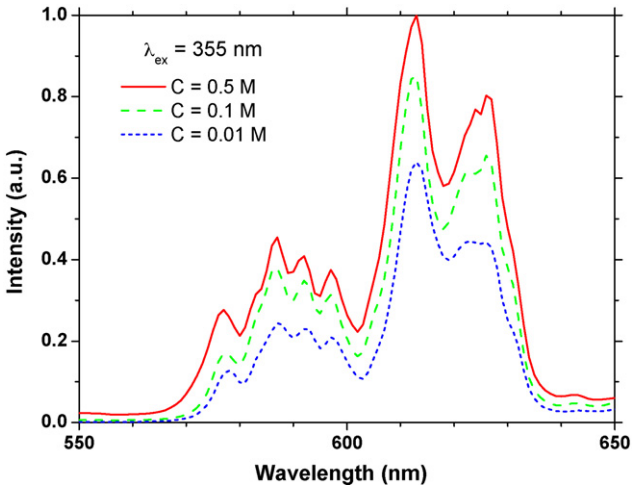

Fig. 9. Emission spectra of as-prepared X_1-Y_2SiO_5 samples from solutions of different overall concentration. Experimental conditions are $\phi = 1.25$ and $x = 0.6$.

4. Conclusions

Nanocrystalline phosphors of europium-doped yttrium silicate (Y_2SiO_5:Eu^{3+}) are successfully synthesized by the flame spray pyrolysis method. These phosphors, having spherical shape, filled morphology, high crystallinity and narrow size distribution, exhibit strong red luminescence. We found that the crystal structure and luminescent intensity

of the as-prepared phosphors are strongly affected by the ratio of silicon to yttrium in the precursor solution. Depending on the silicon (TEOS) concentration, the experiment demonstrates the existence of three different crystal phases: an incomplete X_1-Y_2SiO_5 phase for $\phi < 1.25$, a pure X_1 phase at $1.25 < \phi < 2.0$, and a SiO_2 amorphous structure dominated phase at $\phi > 2.0$. The integral luminescence intensity of the as-prepared and annealed yttrium silicate phosphors is 112% and 126%, respectively, of that of a commercial Y_2O_3:Eu lamp phosphor. The maximum luminescent intensity occurs at a TEOS equivalence ratio of 1.25. Moreover, a concentration quenching limit is observed at a doping concentration of 30 mol% Eu of yttrium. In addition, it is shown that after annealing the X_1-Y_2SiO_5:Eu^{3+} particles at 1300 °C, well-crystallized X_2-type phosphors with stronger PL intensity are obtained. Our work demonstrates the advantages of flame spray pyrolysis method for the preparation of Y_2SiO_5:Eu^{3+} nanophosphor and its potential for industrial applications.

Acknowledgement

Y. Ju would like to thank the support from National Science Foundation via grant DMR-0303947.

References

[1] J. Shmulovich, G.W. Berkstresser, C.D. Brandle, A. Valentino, J. Electrochem. Soc. 135 (1988) 3141.
[2] C. Li, C. Wyon, R. Moncorge, IEEE J. Quantum Electron. 28 (1992) 1209.
[3] M. Jacquemet, F. Balembois, S. Chenais, F. Druon, P. Georges, R. Gaume, B. Ferrand, Appl. Phys. B 78 (2004) 13.
[4] H.H. Busta, Field emission flat displays, in: W. Zhu (Ed.), Vacuum Microelectronics, Wiley/Interscience, New York, 2001.
[5] T.E. Peters, J. Electrochem. Soc. 116 (1969) 985.
[6] X. Ouyang, A.H. Kitai, R. Siegele, Thin Solid Films 254 (1995) 268.
[7] M. Mitsunaga, R. Yano, N. Uesugi, Opt. Lett. 16 (1991) 1890.
[8] J. Ito, H. Johnson, Am. Miner. 53 (1968) 1940.
[9] J. Lin, Q. Su, S. Wang, H. Zhang, J. Mater. Chem. 6 (1996) 265.
[10] N. Taghavinia, G. Lerondel, H. Makino, T. Yao, Nanotechnology 15 (2004) 549.
[11] J.W.M. Verwey, G. Blasse, Mater. Chem. Phys. 25 (1990) 91.
[12] M. Yin, W. Zhang, S. Xia, J.C. Krupa, J. Lumin. 68 (1996) 335.
[13] W. Zhang, P. Xie, C. Duan, K. Yan, M. Yin, L. Lou, S. Xia, J.C. Krupa, Chem. Phys. Lett. 292 (1998) 133.
[14] C.K. Duan, M. Yin, K. Yan, M.G. Reid, J. Alloys Compd. 303–305 (2000) 371.
[15] H. Huang, B. Yan, Solid State Commun. 132 (2004) 773.
[16] Y.C. Kang, I.W. Lenggoro, S.B. Park, K. Okuyama, J. Solid State Chem. 146 (1999) 168.
[17] H.S. Kang, Y.C. Kang, H.D. Park, Y.G. Shul, Appl. Phys. A 80 (2005) 347.
[18] Y.C. Kang, D.J. Seo, S.B. Park, H.D. Park, Jpn. J. Appl. Phys. 40 (2001) 4083.
[19] X. Qin, Y. Ju, S. Bernhard, N. Yao, J. Mater. Res. 20 (2005) 2960.
[20] A. Purwanto, I.W. Lenggoro, H.W. Chang, K. Okuyama, Jpn. J. Chem. Eng. 39 (2006) 68.
[21] D. Dosev, B. Guo, I.M. Kennedy, J. Aerosol Sci. 37 (2006) 402.
[22] H.K. Kammler, L. Mädler, S.E. Pratsinis, Chem. Eng. Technol. 24 (2001) 583.
[23] N.G. Glumac, Y.J. Chen, G. Skandan, B. Kear, Mater. Lett. 34 (1998) 148.
[24] I.W. Lenggoro, T. Hata, F. Iskandar, J. Mater. Res. 15 (2000) 733.
[25] R.J. Kee, J.F. Grcar, M.D. Smooke, J.A. Miller, SANDIA Report SAND85-8240, Sandia National Laboratories, Albuquerque, NM, 1994.
[26] G. Blasse, B.C. Grabmaier, Luminescent Materials, Springer, Berlin, Germany, 1994.
[27] J. Holsa, K. Jyrkas, M. Leskela, J. Less-Common Met. 126 (1986) 215.
[28] P.K. Sharmar, M.H. Jilavi, R. Nass, H. Schmidt, J. Lumin. 82 (1999) 187.
[29] T. Hirai, T. Hirano, I. Komasawa, J. Mater. Chem. 10 (2000) 2306.